



Fermi National Accelerator Laboratory

FERMILAB-Conf-97/313-E

E811

New Measurement of the $P\text{-}\bar{P}$ Total Cross Section at $\sqrt{s} = 1.8$ TeV

C. Avila et al.

*Fermi National Accelerator Laboratory
P.O. Box 500, Batavia, Illinois 60510*

September 1997

Published Proceedings of the *VII Blois Workshop on Elastic and Diffractive Scattering*,
Seoul, Korea, June 10-15, 1997

NEW MEASUREMENT OF THE $P\text{-}\bar{P}$ TOTAL CROSS SECTION AT $\sqrt{s} = 1.8$ TEV

C. AVILA, C. GUSS, M.R. MONDARDINI, J. OREAR

Laboratory of Nuclear Studies, Cornell University, Ithaca, NY 14853, USA

W. BAKER, D. EARTLY, H. JOSTLEIN, S. PRUSS, R. RUBINSTEIN, S. SHUKLA, F. TURKOT

Fermilab, Batavia, IL 60510, USA

R. DESALVO

CERN, Geneva, Switzerland

A new type of detector capable of reaching very small angles was successfully used in Fermilab E811 in Jan. 1996. It consists of a bundle of 15,000 scintillating fibers each of 100 μm diameter. The fibers are oriented parallel to the beam and gave a measuring resolution of 38 μm transverse to the beam. In this report we analysed about 50,000 elastics as close as 3 mm from the beam. Simulated data runs show that the total cross section should be obtained to an accuracy of $\pm 2\%$. The smallest t-bin used has a background subtraction of $\sim 20\%$, but for most of the t-bins the background is much smaller and the detection efficiency is over 95%. Very preliminary analysis gives a total cross section of ~ 71 mb at $\sqrt{s} = 1.8$ TeV using a luminosity-independent method. This is consistent with our earlier Fermilab E710 result which used a different kind of elastic detector. The rho-value analysis has not yet been completed. A personal interpretation (by Orear) of a slower rise in the total cross section is given at the end.

1. Experimental Method

The total $p\bar{p}$ cross section at $\sqrt{s} = 1.8$ TeV is measured using a luminosity-independent method. By definition the total cross section is

$$\sigma_T = \frac{1}{\mathcal{L}} (N_{el}^n + N_{in}) \quad (1)$$

where \mathcal{L} is the integrated luminosity. N_{el}^n is the number of non-coulomb elastics and N_{in} is the number of inelastics. Using the optical theorem, the total cross section can be expressed in terms of the non-coulomb forward differential number of elastics;

$$\sigma_T^2 = \frac{1}{\mathcal{L}} \frac{16\pi(\hbar c)^2}{1+\rho^2} \left. \frac{dN_{el}^n}{dt} \right|_{t=0} \quad (2)$$

Dividing Eq. 2 by Eq. 1 gives

$$\sigma_T = \left[\frac{16\pi(\hbar c)^2}{1+\rho^2} \frac{dN_{el}^n}{dt} \right]_{t=0} \frac{1}{N_{el}^n + N_{in}} \quad (3)$$

Let $\mu = 2\sigma_{sd}/\sigma_{nd}$ where $2\sigma_{sd}$ is the total single diffractive cross section which has been

measured.(1) σ_{nd} is the non-diffractive part of the inelastic cross section. Then after a few steps of algebra one obtains

$$N_{in} = (LR/f)[(1+\mu)/(1+0.05\mu/f)] \quad (4)$$

where $f = 0.896$ is our current estimate of the acceptance of two sets of ring counters on either side of the interaction point for non-diffractive events. LR is the observed coincidence rate. The factor 0.05 is the estimated fraction of single diffractive events that could produce an LR trigger. Because Eqs. 3 and 4 are non-linear, σ_T is obtained by iteration.

The colinear proton and antiproton scattered at angles $\sim 40 \mu\text{rad}$ and above are detected by the scintillating bundle detectors in coincidence on either side of the interaction point.

2. The Detector

In order to have full detector efficiency within ~ 2 mm of the beam we eliminated the usual Roman pot window and mounted the bundle of scintillating fibers inside the beam pipe. The light pattern due to charged particle(s) was conducted outside the beam pipe by a fiber optics rod and amplified by two image intensifiers in series. The screen of the second image intensifier was read out asynchronously by a fast-cleared ccd. Fig. 1 is a plot of digitized voltages per pixel obtained after exposure to a beam halo particle. This region of the screen happened to have a rather large noise pulse. Note that the real particle has an integrated cluster intensity of about 2500 whereas the noise pulse has a reading of about 25; i.e., the signal is about 100 times the background. Detector efficiencies could be measured accurately using redundant triggers. In the last of 9 data taking runs the efficiencies of the light gathering system for our 4 detectors were 0.97, 0.95, 0.99, 0.99. The trigger counter efficiencies were usually above 0.99. More details of the detector are given in Reference (2).

The elastic hardware trigger consists of a left-right coincidence between trigger counters. Colinearity in the xz plane is seen as a diagonal in a XX scatter plot; elastics must also reside on the diagonal in the YY scatter plot. These are shown in Fig. 2 for (a) a large angle run, and for (b) a small angle run. In Fig. 2a there is a uniform beam gas background of about 1%. In Fig. 2b the background due to halo particles increases as one approaches the beam.

3. Preliminary Results

Fig. 3 is a plot of the total nucleon-nucleon cross section vs. s plotted on a log scale. Three values are shown at $\sqrt{s} = 1.8$ TeV: the E710 result of 72.8 ± 3.1 mb(3), the CDF result of 80.3 ± 2.24 mb(4), and a very preliminary value of 71 ± 2 mb for this experiment. This new E811 result agrees with the E710 result. The chi-squared probability that the E811 and CDF results differ as much as they do from their weighted mean is 0.002. It is possible to draw a straight line connecting the E811 result and the points at $\sqrt{s} = 63$ GeV, 540 GeV, and 900 GeV as shown by curve (a). This suggests a $\log(s)$ variation of σ_T with energy.

The local slope of σ_T vs. s can be obtained by evaluating a dispersion relation under the assumption that the p-p and pbar-p cross sections are equal in this energy region:

$$\rho = \frac{\pi s}{2\sigma} \frac{d\sigma}{ds} \quad (5)$$

The slope of curve (a) predicts a value of 0.1 for ρ whereas curve (b) predicts $\rho = 0.25$. The measured value at $\sqrt{s} = 540$ GeV is $\rho = 0.14$ which is consistent with 0.1 and not with 0.25.

4. A Personal Interpretation By the Speaker (Jay Orear)

Could it be that the rise in the total cross section is just a threshold effect? A similar situation is seen in p-p total cross section in the threshold region of pion production (see Fig. 4a). Below the pion threshold there is only elastic scattering due to the well known singlet s-wave

potential. If this contribution were subtracted from the experimental curve in Fig. 4a, there is a rising cross section starting at the pion mass threshold and increasing by ~ 30 mb and then leveling off. This same experimental "curve" is replotted as the solid curve in Fig. 4b. What is plotted is the increase in the cross section as a function of the available energy above threshold. The quantity $\epsilon=0.14$ GeV is used as a scale factor. Now use the experimental value of $\sqrt{s_0}=30$ GeV as the threshold for producing the minijet products of quarks and gluons. Using a scale factor of 300 GeV produces the dashed curve in Fig. 4b which fits the initial rise in the p-p total cross section at the ISR and Fermilab. The UA4, UA5, and E811 points are plotted and show a more gentle rise to the same value of ~ 30 mb. One might expect the production curve for partons of vastly differing masses to be more smeared out than the pion production curve. Certainly there must be a threshold for minijets and that cross section must increase with energy as one moves into the region above threshold. There have been attempts to make a quantitative evaluation of the minijet contribution which seem to agree with the 30 mb rise.⁽⁵⁾

Acknowledgments

This experiment was supported in part by the United States National Science Foundation and the United States Department of Energy. Also we are grateful for support and initial detector development by the small angle subgroup of the LAA Lab at CERN with special help from C. Da Via, M. Lundin, and the director A. Zichichi. We receive invaluable aid from the accelerator, research, and computing divisions at Fermilab.

References

1. N. Amos *et al*, *Phys. Lett.B* 301, 313 (1993), F. Abe *et al*, *Phys. Rev.D.* 50, 5535 (1994)
2. C. Avila *et al*, *Nucl. Instr. and Meth.* A360, 80 (1995)
3. N. Amos *et al*, *Phys. Rev. Letters* 68, 2433 (1992)
4. F. Abe *et al*, *Phys. Rev.D.* 50, 5550 (1994)
5. T.K. Gaisser and F. Halzen, *Phys. Rev. Letters* 16, 1754 (1985)..

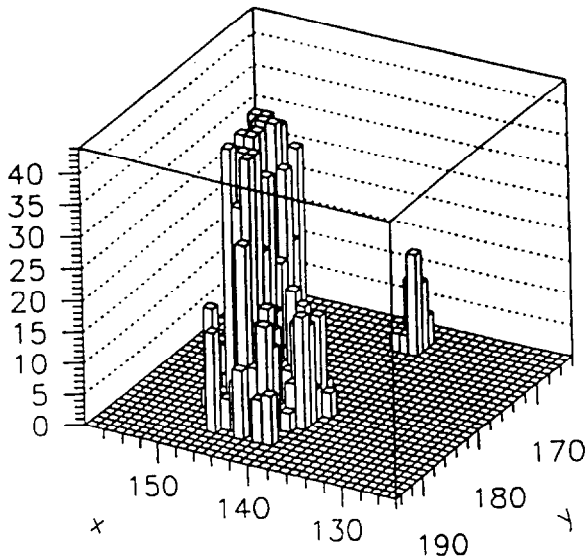


Figure 1: Pixel intensity for a real particle cluster compared to a rather large and nearby noise cluster.

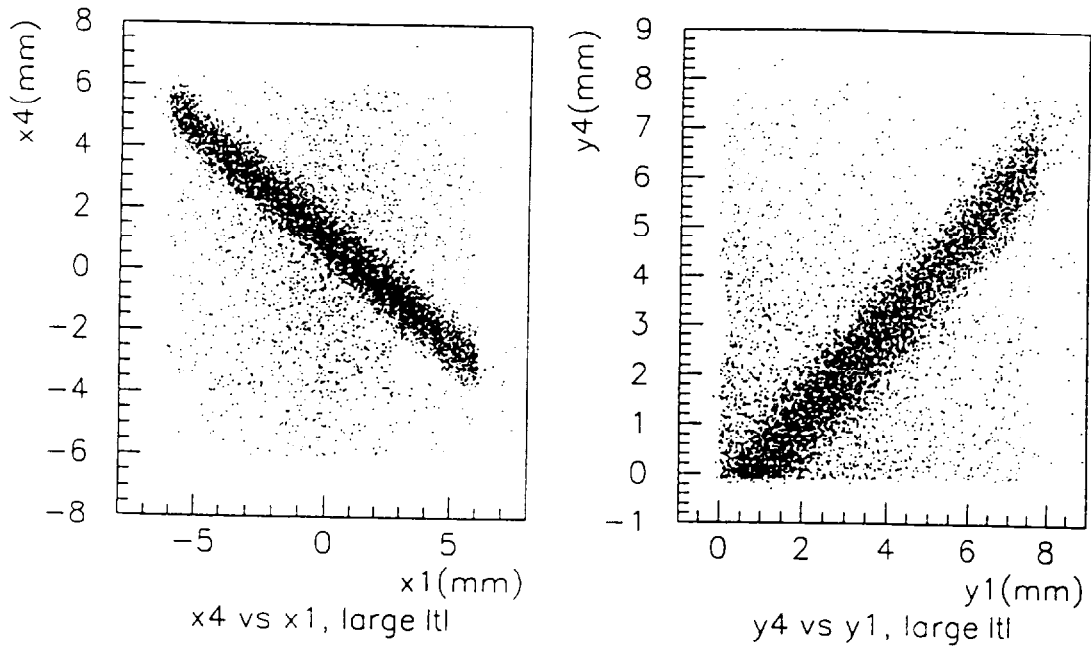


Figure 2a: XX and YY scatterplots for elastic detectors 8.3 mm from the beam.

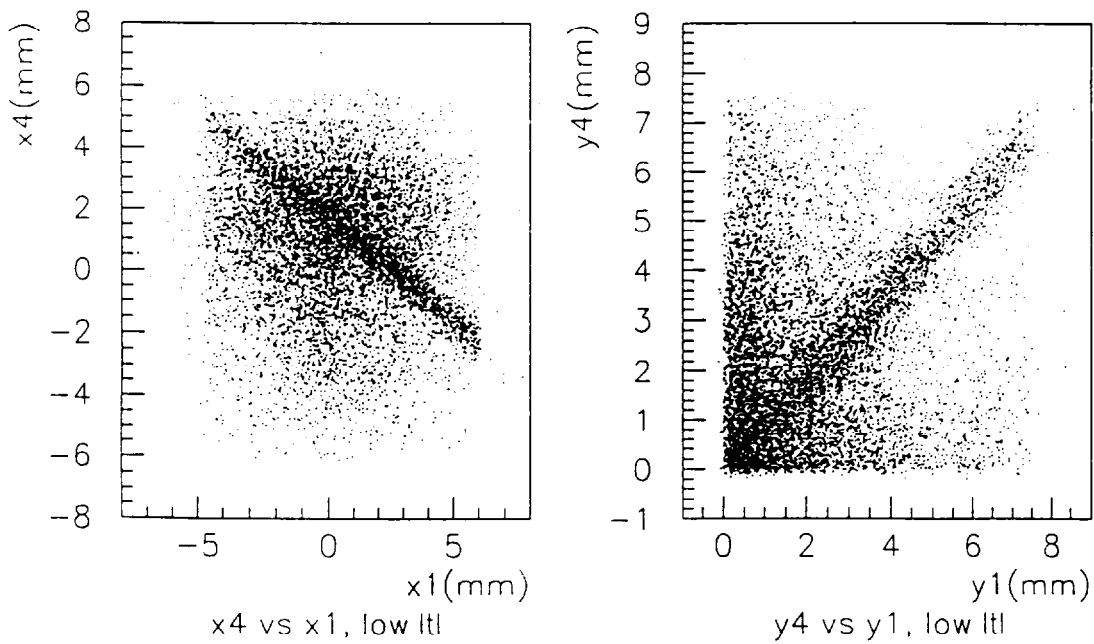


Figure 2b: XX and YY scatterplots for elastic detectors 2.8 mm from the beam.

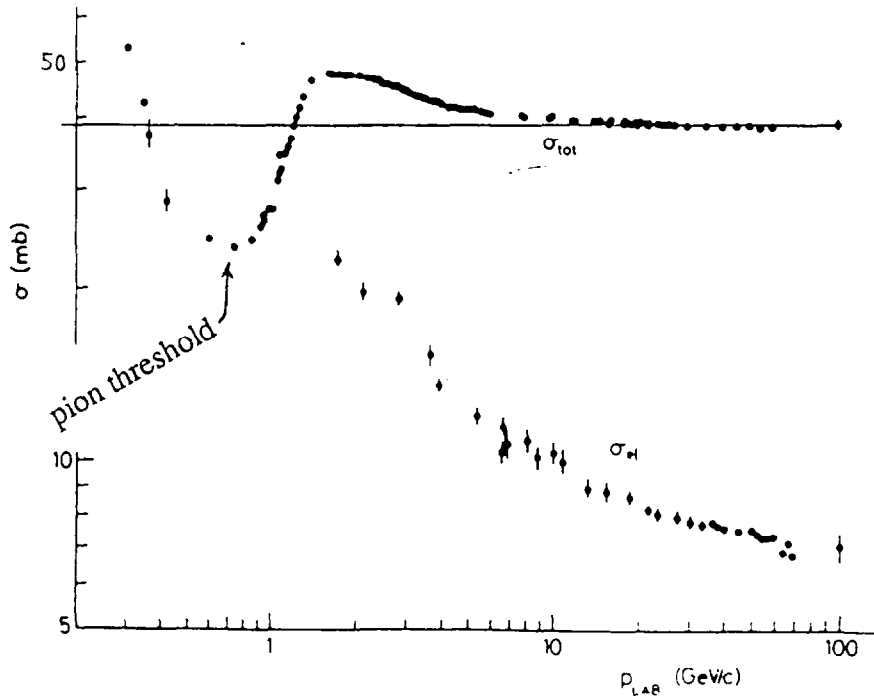
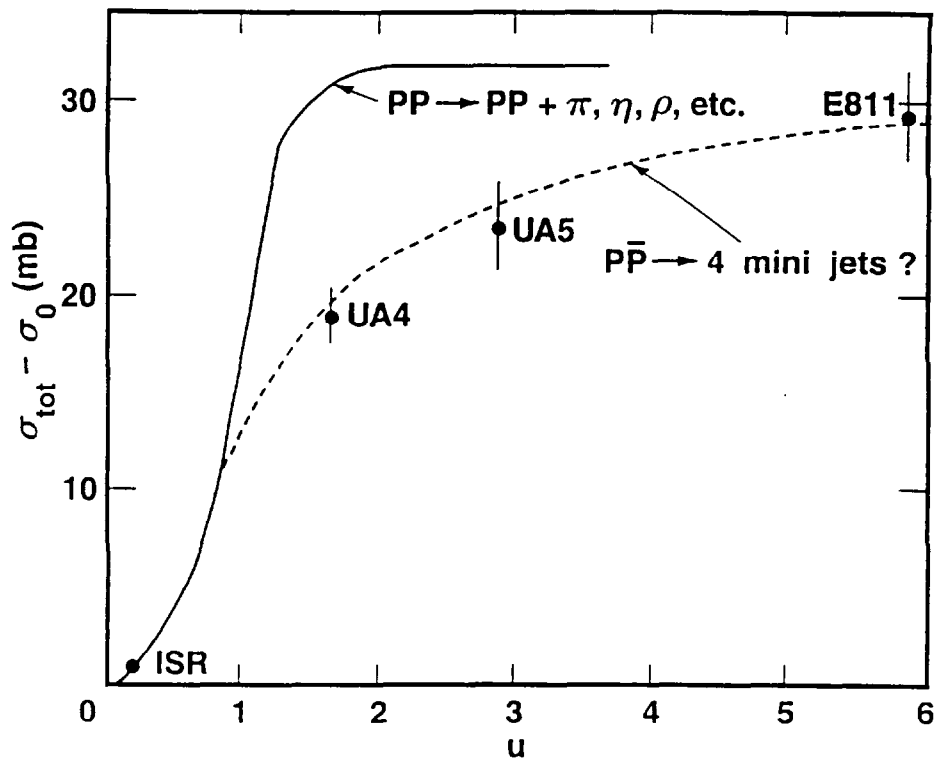


Figure 4a: PP total and elastic cross sections in the pion threshold region.



For $\sqrt{s} < 30$ GeV: $\sqrt{s_0} = (2Mc^2 + 0.14 \text{ GeV})$ and $\epsilon = .14$ GeV.

For $\sqrt{s} > 30$ GeV: $\sqrt{s_0} = 30$ GeV and $\epsilon = 300$ GeV.

Figure 4b: The solid curve is a replot of the experimental curve in Fig. 4a as a function of u where $u = (\sqrt{s} - \sqrt{s_0})/\epsilon =$ (energy above threshold)/(scale factor ϵ). The dashed curve is a smooth connecting of the high energy experimental points plotted using a threshold of 30 GeV and $\epsilon = 300$ GeV.